

Dense Correspondence of Skull Models by Automatic Detection of Anatomical Landmarks

Kun Zhang, Yuan Cheng, and Wee Kheng Leow

Department of Computer Science, National University of Singapore
Computing 1, 13 Computing Drive, Singapore 117417
zhangkun cyuan leowwk@comp.nus.edu.sg

Abstract. Determining dense correspondence between 3D skull models is a very important but difficult task due to the complexity of the skulls. Non-rigid registration is at present the predominant approach for dense correspondence. It registers a reference model to a target model and then resamples the target according to the reference. Methods that use manually marked corresponding landmarks are accurate, but manual marking is tedious and potentially error prone. On the other hand, methods that automatically detect correspondence based on local geometric features are sensitive to noise and outliers, which can adversely affect their accuracy. This paper presents an automatic dense correspondence method for skull models that combines the strengths of both approaches. First, anatomical landmarks are automatically and accurately detected to serve as hard constraints for non-rigid registration. They ensure that the correspondence is anatomically consistent and accurate. Second, control points are sampled on the skull surfaces to serve as soft constraints for non-rigid registration. They provide additional local shape constraints for a closer match between the reference and the target. Test results show that, by combining both approaches, our algorithm can achieve more accurate automatic dense correspondence.

Keywords: Dense correspondence, anatomical landmarks, skull models

1 Introduction

Determining dense correspondence between 3D mesh models is a very important task in many applications such as remeshing, shape morphing, and construction of active shape models. Among existing approaches for dense correspondence, non-rigid registration is at present the predominant approach due to its flexibility. Non-rigid registration methods deform a reference mesh to match the target mesh and resample the target by mapping reference mesh vertices to the target surface. They are typically preceded by rigid registration to globally align the sizes, positions, and orientations of the meshes. Various deformable methods have been used including energy minimization [11, 12], mass-spring model [15], local affine transformations [1], trilinear transformation [2], graph and manifold matching [20], octree-splines [6], and thin-plate spline (TPS) [4, 5, 7–10, 14, 18].

Most of these methods are demonstrated on models with simple surfaces such as faces [8, 12, 20], human bodies [1, 15], knee ligaments [6], and lower jaws [2]. TPS is particularly effective for mesh models with highly complex surfaces such as brain sulci [4], lumbar vertebrae [10], and skulls [5, 7, 9, 14, 18]. Skull models are particularly complex because they have holes, missing teeth and bones, and interior as well as exterior surfaces.

Like all non-rigid registration methods, TPS registration of skull models requires known correspondence on the reference and the target, which can be manually marked or automatically detected. The first approach manually marks anatomical landmarks on the reference and the target [5, 9, 14], and uses the landmarks as hard constraints in TPS registration. This approach is accurate, but manual marking is tedious and potentially error prone. The second approach automatically detects surface points on the reference mesh, which are mapped to the target surface. These surface points can be randomly sampled points [7] or distinctive feature points such as local curvature maximals [18], and they serve as soft constraints in TPS registration. This approach is sensitive to noise, outliers, and false correspondences. Turner et al. [18] apply multi-stage coarse-to-fine method to reduce outliers, and forward (reference-to-target) and backward (target-to-reference) registrations to reduce false correspondences. However, there is no guarantee that the correspondences detected anatomically are consistent and accurate, despite the complexity of the method.

This paper presents an automatic dense correspondence algorithm for skull models that combines the strengths of both approaches. First, anatomical landmarks are automatically and accurately detected to serve as hard constraints in TPS registration. They ensure **anatomically consistent correspondence**. The number of such landmarks is expected to be small because automatic detection of anatomical landmarks is a very difficult task (Section 2). Second, control points are sampled on skull surfaces to serve as soft constraints in TPS registration. They provide additional local shape constraints for a **close matching** of reference and target surfaces. Compared to [18], our method also uses multi-stage coarse-to-fine approach, except that our landmark detection algorithm is based on anatomical definitions of landmarks, which ensures the correctness and accuracy of the detected landmarks.

Quantitative evaluation of point correspondence is a challenging task. Most works reported only qualitative results. The quantitative errors measured in [2, 8, 19] are non-rigid registration error instead of point correspondence error. This paper proposes a method for measuring point correspondence error, and shows that registration error is not necessarily correlated to correspondence error.

2 Automatic Craniometric Landmark Detection

In anatomy [16] and forensics [17], craniometric landmarks are feature points on a skull that are used to define and measure skull shapes. Automatic detection of craniometric landmarks is very difficult and challenging due to a form of cyclic definition. Many craniometric landmarks are defined according to the three

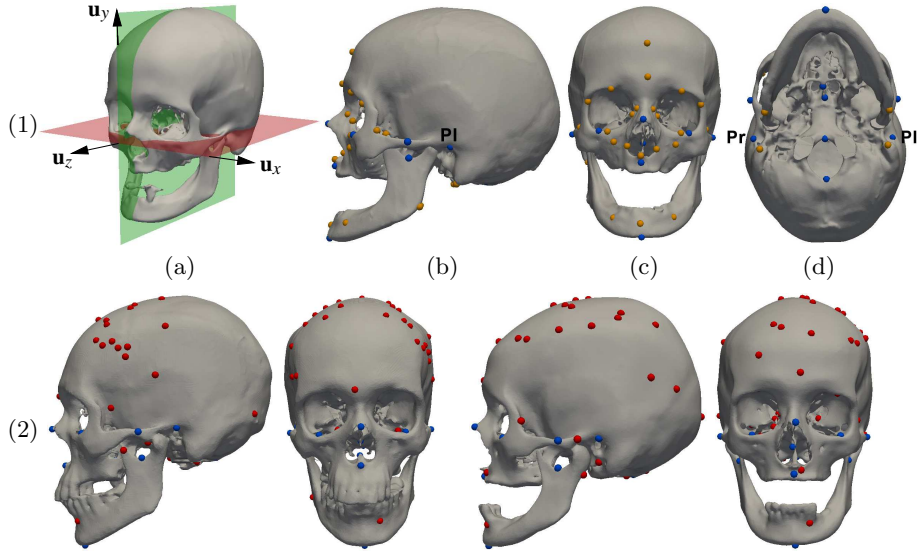


Fig. 1. Skull models and craniometric landmarks. (1) Reference model. (1a) Frankfurt plane (FP) is the horizontal (red) plane and mid-sagittal plane (MSP) is the vertical (green) plane. (1b–1d) Blue dots denote landmarks used for registration and yellow dots denote Landmarks used for evaluation. (2) Detected registration landmarks (blue) and 50 control points (red) on two sample test targets.

anatomical orientations of the skull (Fig. 1(a)): lateral (left-right), anterior-posterior (front-back), and superior-inferior (up-down). These orientations are defined by the *Frankfurt plane* (FP) and the *mid-sagittal plane* (MSP), which are in turn defined as the planes that pass through specific landmarks.

Our automatic landmark detection algorithm is an adaptation of our previous work on automatic identification of FP and MSP [3]. It overcomes the cyclic definition of craniometric landmarks by first mapping known landmarks on a reference model to a target model, and then iteratively refining FP, MSP and their landmarks on the target model. It can be summarized as follows:

Craniometric Landmark Detection Algorithm

1. Register a reference model with known landmarks to the target model.
2. Locate the landmarks on the target based on the registered reference and fit FP and MSP to their landmarks on the target.
3. Repeat until convergence:
 - (a) Refine the locations of the FP landmarks on the target, and fit FP to the refined FP landmarks.
 - (b) Refine the locations of the MSP landmarks on the target, and fit MSP to the refined MSP landmarks, keeping it orthogonal to FP.

Step 1 registers the reference to the target using Fractional Iterative Closest Point (FICP) [13], a variant of ICP robust to noise, outliers, and missing bones.

Like ICP, FICP iteratively computes the best similarity transformation (scaling, rotation, and translation) that registers the reference to the target. The difference is that in each iteration, FICP computes the transformation using only a subset of reference points whose distances to the target model are the smallest.

After registration, Step 2 maps the landmarks on the reference to the target. First, closest points on the target surface to the reference landmarks are identified. These closest points are the initial estimates of the landmarks on the target, which may not be accurate due to shape variations among the skulls. Next, FP and MSP are fitted to the initial estimates using PCA.

In Step 3, an elliptical landmark region R is identified around each initial estimate. The orientation and size of R are empirically predefined. R varies for different landmark according to the shape of the skull around the landmark. These regions should be large enough to include the landmarks on the target model. Accurate landmark locations are searched within the regions according to their anatomical definitions. For example, the left and right porions (Pl, Pr in Fig. 1) are the most *lateral* points of the roofs of the ear canals [16, 17]. After refining FP landmarks in Step 3(a), FP is fitted to the refined FP landmarks. Next, MSP landmarks are refined in Step 3(b) in a similar manner, and MSP is fitted to the refined MSP landmarks, keeping it orthogonal to FP.

As Step 3 is iterated, the locations and orientations of FP and MSP are refined by fitting to the landmarks, and the landmarks' locations are refined according to the refined FP and MSP. After the algorithm converges, accurate craniometric landmarks are detected on the target model.

In addition to the landmarks on FP and MSP, other landmarks are also detected (Fig. 1). These include points of extremum along the anatomical orientations defined by FP and MSP. These landmarks are detected in a similar manner as the FP and MSP landmarks, first by mapping known landmark regions on the reference to the target, and then searching within the regions for the landmarks according to their anatomical definitions. Test results show that the average landmark detection error is 3.54 mm, which is very small compared to the size of human skulls.

3 Dense Correspondence Algorithm

Our dense correspondence algorithm consists of the following stages:

1. Apply craniometric landmark detection algorithm on the target model.
2. Apply TPS to register the reference to the target with craniometric landmarks as hard constraints.
3. Sample control points on reference surface and map them to target surface.
4. Apply TPS with craniometric landmarks as hard constraints and control points as soft constraints.
5. Resample target surface by mapping reference mesh vertices to the target.

Stage 1 automatically detects craniometric landmarks on the target model. After applying the landmark detection algorithm, the reference model is already rigidly registered to the target model. Stage 2 applies TPS to perform coarse

registration with the accurately detected landmarks as hard constraints, which ensure **anatomically consistent correspondence**. Stage 3 randomly selects m reference mesh vertices with the large registration errors as the control points. For each control point, a nearest point on the target surface within a fixed distance and with a sufficiently similar surface normal is selected as the corresponding point. If a corresponding point that satisfies these criteria cannot be found, then the control point is discarded. This approach renders the algorithm robust to missing parts in the target skulls. Stage 4 performs another TPS registration with craniometric landmarks as hard constraints and control points as soft constraints. These constraints ensure **close matching** of reference and target surfaces while maintaining anatomically consistent correspondence. After TPS registration, Stage 5 maps the reference mesh vertices to the target surface in the same manner as mapping of control points in Stage 3.

4 Accuracy of Registration and Correspondence

Registration error E_R measures the difference between the registered reference surface and the target surface. It can be computed as the mean distance between the reference mesh vertices \mathbf{v}_i^r and the nearest surface points \mathbf{v}_i^t on the target:

$$E_R = \left[\frac{1}{n} \sum_{i=1}^n \|\mathbf{v}_i^r - \mathbf{v}_i^t\|^2 \right]^{1/2} \quad (1)$$

where n is the number of vertices. This is essentially the error measured in [2, 8, 19], although the actual formulations that they used differ slightly.

Correspondence error, on the other hand, should measure the error in computing point correspondence. One possible formulation of correspondence error is to measure the mean distance between the desired and actual corresponding target points of reference mesh vertices. The desired corresponding point $D(\mathbf{v}_i^r)$ is the ground-truth marked by a human expert, whereas the actual corresponding point $C(\mathbf{v}_i^r)$ is the one computed by dense correspondence algorithm. With this formulation, the correspondence error E_C can be computed as

$$E_C = \left[\frac{1}{n} \sum_{i=1}^n \|D(\mathbf{v}_i^r) - C(\mathbf{v}_i^r)\|^2 \right]^{1/2} \quad (2)$$

In practice, it is impossible to manually mark the desired corresponding points of reference mesh vertices accurately on the target mesh surface. An alternative formulation is to measure the mean distance between the desired and actual corresponding target landmarks of reference landmarks \mathbf{M}_i^r :

$$E_C = \left[\frac{1}{l} \sum_{i=1}^l \|D(\mathbf{M}_i^r) - C(\mathbf{M}_i^r)\|^2 \right]^{1/2} \quad (3)$$

where l is the number of evaluation landmarks. The desired target landmarks are manually marked whereas the actual target landmarks are computed by

the dense correspondence algorithm. Given enough landmarks adequately distributed over the entire reference surface, Eq. 3 is a good approximation of Eq. 2.

5 Experiments and Discussions

11 skull models reconstructed from CT images were used in the tests. One of them served as the reference model and the others were target models. For performance comparison, the following methods were tested for dense correspondence:

1. ICP: ICP rigid registration with mesh vertices as corresponding points.
2. FICP: FICP rigid registration with mesh vertices as corresponding points.
3. CP-S: TPS registration with automatically detected control points as soft constraints. This approach was adopted by [7].
4. LM-H: TPS registration with automatically detected craniometric landmarks as hard constraints.
5. LM-S/CP-S: TPS registration with automatically detected craniometric landmarks and control points as soft constraints. This approach is similar to the method of [18], except [18] adopted a more elaborate multi-stage, coarse-to-fine, and forward-backward registration scheme.
6. **LM-H/CP-S**: TPS registration with automatically detected craniometric landmarks as hard constraints and control points as soft constraints. This is our proposed algorithm.
7. MLM-H: TPS registration with manually marked craniometric landmarks as hard constraints. This approach was adopted by [5, 9, 14].

These test cases were equivalent to our algorithm (Case 6) with different stages and constraints omitted. All the TPS registrations were preceded by FICP. The stiffness parameter for TPS soft constraints was set to 0.8 where the algorithms generally performed well. 15 landmarks and 150 control points were used for registration for Cases 3–6, and 30 landmarks for Case 7. More landmarks could be used for Case 7 because they included landmarks that could be accurately marked manually but not detected automatically. 28 other landmarks were used for evaluation. Both registration error and correspondence error were measured.

Test results (Figure 2(a)) show that FICP is more robust than ICP in rigid registration. The registration error of CP-S is smaller than those of LM-S/CP-S and LM-H/CP-S, but its correspondence error is larger. This shows that low registration error does not necessarily imply low correspondence error.

CP-S and LM-S/CP-S use only soft constraints, which are inadequate for ensuring anatomically consistent correspondence. So, their correspondence errors are larger than those of LM-H/CP-S, which also uses registration landmarks as hard constraints. On the other hand, LM-H uses only landmarks, which are insufficient for ensuring close matching of reference and target surfaces, though consistent correspondence is somewhat achieved. So, its correspondence error for registration landmarks E_{CR} is very small, but its correspondence error for evaluation landmarks E_{CE} is large. LM-S/CP-S uses landmarks as soft constraints, which weakens the anatomical consistency of correspondence, though close matching of reference and target surfaces is achieved. Using landmarks as

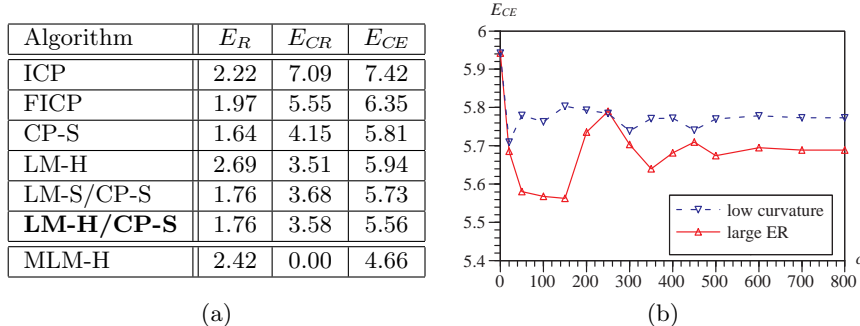


Fig. 2. Quantitative evaluation. (a) E_R : registration error. E_{CR} , E_{CE} : correspondence errors for registration landmarks and evaluation landmarks, respectively. Units are in mm. (b) Plots of E_{CE} vs. c , number of control points.

hard constraints, our algorithm LM-H/CP-S ensures strong anatomically consistent correspondence. Together with control points as soft constraints, it achieves very low registration error and the lowest correspondence error for evaluation landmarks E_{CE} among the automatic methods (Cases 1–6).

MLM-H uses manually marked landmarks as hard constraints. So, it is not surprising that it has the smallest correspondence errors. Interestingly, its registration error is quite large compared to the other methods. This is because some parts of the skulls lack distinctive surface features for locating both registration and evaluation landmarks (Fig. 1), where most of the registration errors occur.

To investigate the stability of our algorithm LM-H/CP-S, we tested it with varying numbers of control points and two different sampling schemes that are used by existing methods: low curvature [18] and large registration error [5]. Figure 2(b) shows that control points with large registration errors are more effective than those with low curvatures in reducing correspondence error. Compared to the accuracy of LM-H, which uses landmarks only, a small number of control points can already improve correspondence accuracy significantly. After sampling enough control points that cover various parts of the skulls, adding more control points do not reduce correspondence error significantly. This is due to the diminished quality of the additional control points.

6 Conclusions

This paper presents a multi-stage, coarse-to-fine automatic dense correspondence algorithm for mesh models of skulls that combines two key features. First, anatomical landmarks are automatically and accurately detected to serve as hard constraints for non-rigid registration. They ensure **anatomically consistent correspondence**. Second, control points are sampled on the skull surfaces to serve as soft constraints for non-rigid registration. They provide additional local shape constraints to ensure **close matching** of reference and target surfaces. Test results show that, by combining both approaches, our algorithm can

achieve more accurate automatic dense correspondence than other automatic algorithms. Our test results also show that low registration error does not always imply low correspondence error. So, both error measures should be used in conjunction to evaluate the accuracy of dense correspondence algorithms.

References

1. B. Allen, B. Curless, and Z. Popović. The space of human body shapes: reconstruction and parameterization from range scans. In *Proc. SIGGRAPH*, 2003.
2. M. Berar, M. Desvignes, G. Bailly, and Y. Payan. 3D meshes registration: Application to statistical skull model. In *Proc. Image Analysis and Recognition*, 2004.
3. Y. Cheng, W. K. Leow, and T. C. Lim. Automatic identification of frankfurt plane and mid-sagittal plane of skull. In *Proc. WACV*, 2012.
4. H. Chui and A. Rangarajan. A new algorithm for non-rigid point matching. In *Proc. CVPR*, 2000.
5. Q. Deng, M. Zhou, W. Shui, Z. Wu, Y. Ji, and R. Bai. A novel skull registration based on global and local deformations for craniofacial reconstruction. *Forensic Science International*, 208:95–102, 2011.
6. M. Fleute and S. Lavallée. Building a complete surface model from sparse data using statistical shape models: Application to computer assisted knee surgery. In *Proc. MICCAI*, 1998.
7. Y. Hu, F. Duan, M. Zhou, Y. Sun, and B. Yin. Craniofacial reconstruction based on a hierarchical dense deformable model. *EURASIP Journal on Advances in Signal Processing*, 217:1–14, 2012.
8. T. J. Hutton, B. F. Buxton, and P. Hammond. Automated registration of 3D faces using dense surface models. In *Proc. BMVC*, 2003.
9. R. J. A. Lapeer and R. W. Prager. 3D shape recovery of a newborn skull using thin-plate splines. *Computerized Medical Imaging & Graphics*, 24(3):193–204, 2000.
10. C. Lorenz and N. Krahnstöver. Generation of point-based 3D shape models for anatomical objects. *Computer Vision and Image Understanding*, 77:175–191, 2000.
11. M. Lüthi, T. Albrecht, and T. Vetter. Building shape models from lousy data. In *Proc. MICCAI*, 2009.
12. G. Pan, S. Han, Z. Wu, and Y. Zhang. Removal of 3D facial expressions: A learning-based approach. In *Proc. CVPR*, 2010.
13. J. M. Phillips, R. Liu, and C. Tomasi. Outlier robust icp for minimizing fractional RMSD. In *Proc. 3D Digital Imaging and Modeling*, 2007.
14. A. Rosas and M. Bastir. Thin-plate spline analysis of allometry and sexual dimorphism in the human craniofacial complex. *American J. Physical Anthropology*, 117:236–245, 2002.
15. H. Seo and N. Magnenat-Thalmann. An automatic modeling of human bodies from sizing parameters. In *Proc. ACM SIGGRAPH*, 2003.
16. D. F. Siwek and R. J. Hoyt. Anatomy of the human skull. <http://skullanatomy.info>.
17. K. T. Taylor. *Forensic Art and Illustration*. CRC, 2001.
18. W. D. Turner, R. E. Brown, T. P. Kelliher, P. H. Tu, M. A. Taister, and K. W. Miller. A novel method of automated skull registration for forensic facial approximation. *Forensic Science International*, 154:149–158, 2005.
19. Y. Wang, B. S. Peterson, and L. H. Staib. Shape-based 3D surface correspondence using geodesics and local geometry. In *Proc. CVPR*, 2000.
20. Y. Zeng, C. Wang, and Y. Wang. Dense non-rigid surface registration using high-order graph matching. In *Proc. CVPR*, 2010.